

Cite this: *J. Mater. Chem. A*, 2014, 2, 6167

Mussel-inspired nitrogen-doped graphene nanosheet supported manganese oxide nanowires as highly efficient electrocatalysts for oxygen reduction reaction†

Taemin Lee, Eun Kyung Jeon and Byeong-Su Kim*

Electrocatalysts for oxygen reduction reaction (ORR) play a vital role in determining the performance of fuel cells and metal–air batteries. Carbon nanomaterials doped with heteroatoms are highly attractive by virtue of their excellent electrocatalytic activity, high conductivity and large surface area. This study reports the synthesis of a highly efficient electrocatalyst based on nitrogen-doped (N-doped) graphene nanosheets (NG) using mussel-inspired dopamine as a nitrogen source. Dopamine undergoes oxidative polymerization that can functionalize the surface of graphene and also introduces nitrogen atoms onto the graphene nanosheets upon pyrolysis. N-doping not only leads to improved catalytic activity, but it also provides anchoring sites for the growth of electroactive amorphous manganese oxide nanowires on the graphene nanosheets (NG/MnO_x). On the basis of a Koutecky–Levich plot, it is found that the hybrid NG/MnO_x catalyst exhibits excellent catalytic activity with a direct four-electron pathway in ORR. Furthermore, the hybrid electrocatalyst possesses superior stability and gives a low yield of peroxide compared to commercial Pt/C catalysts. This suggests that the unique combination of an N-doped graphene support and amorphous MnO_x nanowires can synergistically improve the catalytic activity for ORR.

Received 16th October 2013
Accepted 29th November 2013

DOI: 10.1039/c3ta14147k

www.rsc.org/MaterialsA

Introduction

Nature has been a constant source of inspiration for the design of novel materials for a variety of advanced applications. Inspired by the unusual amino acid 3,4-dihydroxy-L-phenylalanine, dopamine, found in the adhesive pads of mussels, herein a simple solution-based surface functionalization of dopamine on the graphene nanosheets is reported. Dopamine serves as a source of nitrogen-doping (N-doping) and as an anchoring site for the growth of the manganese oxide (MnO_x) nanostructure, providing highly efficient electrocatalysts for oxygen reduction reaction (ORR).

Increasing energy demands, coupled with the limited availability of fossil fuels and their associated environmental issues, have stimulated intense research on energy storage and conversion systems.^{1–4} Although lithium ion batteries are the leading choice for energy storage today, they cannot sufficiently satisfy long-term storage requirements due to the inherent limitation of gravimetric energy density to meet

various energy demands.^{2,5,6} Alternatively, fuel cells and metal–air batteries have recently received attention as promising power sources because of their remarkable theoretical energy density, and environmental benignity.^{1,7–11} Despite their promising features, their use in various fields is still limited owing to their sluggish kinetics and irreversible electrochemical redox reactions. As a consequence, the activity of electrocatalysts for cathodic ORR plays a vital role in determining the electrochemical performance of alkaline fuel cells and metal–air batteries.^{12–15} In that regard, many noble metal catalysts, such as Pt and Pt-based alloys, have been widely employed as ORR catalysts owing to their excellent catalytic efficiency, relatively low overpotential, and high current density.^{12,16–18} Nonetheless, they still suffer from multiple limiting factors, including intermediate tolerance, anode crossover, sluggish kinetics, and poor stability together with their high cost and limited reserves, which have restricted their use for large-scale applications.^{19–21} Therefore, the search for alternative catalysts has led to the recent development of non-precious metal catalysts and metal-free carbon nanomaterials.^{13,14,22–26} Among them, MnO_x is a particularly attractive candidate because of its high catalytic activity, high abundance, high stability, low cost, and minimal environmental issues.^{27–33} However, there are still obstacles in utilizing MnO_x as an efficient ORR catalyst as it has an intrinsically low electrical conductivity.^{34–36}

Interdisciplinary School of Green Energy and Department of Chemistry, Ulsan National Institute of Science and Technology (UNIST), Ulsan 689-798, Korea. E-mail: bskim19@unist.ac.kr

† Electronic supplementary Information (ESI) available: UV/vis spectrum, relative atomic contents and deconvoluted peak information from the XPS study, thermogravimetric analysis (TGA), and additional electrochemical analysis for TRGO and NG/MnO_x catalysts. See DOI: 10.1039/c3ta14147k

Graphene, a monolayer of aromatic carbon lattice, has recently drawn tremendous interest owing to its extraordinary electrical, optical, thermal, and mechanical properties.^{37–39} Taking full advantage of its chemical stability and high conductivity along with its high specific surface area, graphene nanosheets and their heteroatom-doped structures offer promising opportunities for ORR catalysts.^{40,41} In addition, graphene nanosheets are excellent substrates for hosting and growing functional nanomaterials for high-performance electrochemical and electrocatalytic devices.^{42–50} In general, N-doped graphenes are commonly prepared by several methods, including chemical vapor deposition in the presence of a nitrogen source,⁵¹ thermal annealing with ammonia,⁵² pyrolysis of a nitrogen-containing precursor (such as melamine, polypyrrole, and pyridine),^{53–56} and nitrogen-plasma treatments of graphene.⁵⁷ These approaches facilitate successful introduction of nitrogen atoms within the graphene nanosheets, which provide active sites for ORR, resulting in increased electrocatalytic activity. However, many of these approaches require toxic gas precursors, or it is difficult to control the degree of doping and type of nitrogen functionality.

Herein, a novel design of N-doped graphene nanosheets (NG) by integration of the robust, mussel-inspired chemical motif of dopamine is developed (Fig. 1). Dopamine serves as a source of nitrogen and an anchoring site for the growth of MnO_x nanowires on the surface of graphene nanosheets. It was found that the N-doping effectively contributed to enhanced electrocatalytic activity in comparison with its non-doped counterpart. Furthermore, the integration of MnO_x nanowires onto NG nanosheets *via* a solution-based approach afforded hybrid NG/MnO_x catalysts that preserved an even higher electrocatalytic efficiency with a low yield of peroxide and good durability through an efficient one-step, four-electron pathway similar to commercial Pt/C catalysts.

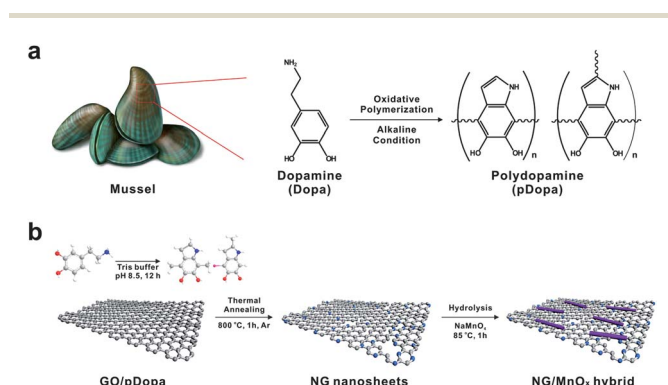


Fig. 1 (a) Chemical structures of dopamine (Dopa) from the adhesive protein found in mussel pads and its polymerized polydopamine (pDopa) under alkaline conditions. (b) Schematic representation of the synthesis of hybrid manganese oxide nanowires supported on nitrogen-doped graphene nanosheets (NG/MnO_x) as highly efficient electrocatalysts for oxygen reduction reaction.

Experimental

Preparation of graphene oxide (GO) suspension

Graphite oxide was synthesized from graphite powder (Aldrich, <20 μm) by the modified Hummers method and exfoliated to give a brown dispersion of graphene oxide (GO) under ultrasonication. The GO powder, dissolved in a known volume of water, was subjected to ultrasonication for 40 min to give a stable suspension of GO (typical conc. of 0.50 mg mL⁻¹) and then centrifuged at 4000 rpm for 10 min to remove any aggregates remaining in the suspension.

Preparation of non-doped graphene catalysts

Chemically reduced GO (CRGO) was prepared by reacting 50 mL of as-prepared GO suspension (conc. 0.50 mg mL⁻¹) with 10 μL of a 35 wt% hydrazine solution and 70 μL of an ammonia solution. Then, this mixture was stirred at 95 °C for 1 h to afford CRGO. Thermally reduced GO (TRGO) was prepared by placing pristine GO powder into a tube furnace, heating it up to 800 °C at a heating rate of 10 °C min⁻¹ and maintaining for 1 h in an Ar atmosphere.

Preparation of N-doped graphene (NG) catalysts

To prepare the dopamine functionalized graphene nanosheets (G/pDopa), 20 mL of an aqueous suspension of GO (conc. 0.5 mg mL⁻¹) was mixed with a dopamine suspension (conc. 2 mg mL⁻¹ dispersed in 10 mM Tris buffer, pH 8.5) and stirred at room temperature overnight. The sample was then collected using a nylon membrane filter (0.20 μm pore size, Corning, USA), washed with deionized water several times, and dried by lyophilization. The resulting G/pDopa powder was annealed in a quartz-tube furnace at different temperatures from 600 to 1000 °C to achieve pyrolysis of the polydopamine. After the temperature was maintained for 1 h, the furnace was cooled down to room temperature slowly to recover the NG catalysts.

Preparation of hybrid NG/MnO_x catalysts

The as-prepared NG powder was dispersed in DMF at a specific concentration (conc. 0.50 mg mL⁻¹). The Mn precursor, NaMnO₄, was then added to the NG suspension at various feed ratios (the ratio of NG to Mn precursor ranged from 0.5 to 10). The mixture was heated to 85 °C for 1 h, collected by centrifugation followed by washing with solvent several times and dried in a vacuum oven.

Preparation of catalyst ink for the rotating disk electrode

2.0 mg of the as-prepared catalyst was dispersed in 1.0 mL of the mixture solvent with Nafion (5 wt% dispersed in IPA) in a specific volume ratio (H₂O : DMF : Nafion = 8 : 1 : 1). Catalyst ink was prepared by ultrasonically mixing for 1 h to obtain a homogeneous suspension. Then, 5 μL of the prepared catalytic ink was transferred to the surface of the 3 mm diameter glassy carbon electrode using a micropipette. Finally, the ink was dried for 10 min under vacuum conditions at room temperature to form a thin catalyst film on the glassy carbon electrode as a working electrode.

Exploration of the ORR kinetics of catalysts based on the Koutecky–Levich equation

To explore the ORR and the related kinetics, the Koutecky–Levich (K–L) equation was used to transform the data obtained from rotating-disk electrode (RDE) experiments.^{68,69} The linearity of the K–L plots and near parallelism of the fitting lines suggest first-order reaction kinetics for the concentration of dissolved oxygen and similar electron transfer numbers for ORR at different potentials.

$$\frac{1}{i} = \frac{1}{i_k} + \frac{1}{i_{dl}} = \frac{1}{i_k} + \frac{1}{B\omega^{0.5}} \quad (1)$$

$$i_k = nFAkC_{O_2} \text{ (kinetic current)} \quad (2)$$

$$i_{dl} = 0.20nFAC_{O_2}D_{O_2}^{2/3}\nu^{-1/6}\omega^{1/2} \text{ (diffusion limiting current)} \quad (3)$$

where i_k represents the kinetic current, i_{dl} is the diffusion limiting current, n is the number of electrons transferred per O_2 molecule, F is the Faraday constant (96485 C mol^{-1}), A is the geometric area of the disk electrode ($7.06 \times 10^{-6} \text{ m}^2$), k (m s^{-1}) is the rate constant for the ORR, C_{O_2} is the saturated concentration of O_2 in solution (1.21 mol m^{-3} in 0.10 M KOH), ν is the kinematic viscosity ($1 \times 10^{-6} \text{ m}^2 \text{ s}^{-1}$ in 0.10 M KOH), D_{O_2} is the diffusion coefficient of O_2 in solution ($1.87 \times 10^{-9} \text{ m}^2 \text{ s}^{-1}$ in 0.10 M KOH), and ω is the angular frequency of the rotation (rad s^{-1}). From the linear relationship between i^{-1} and $\omega^{-0.5}$ based on the K–L equation, one can obtain the number of electrons transferred (n) from the slope and the kinetic current (i_k) from the intercept.

Rotating ring disk electrode (RRDE) experiment

Rotating ring disk electrode (RRDE) (ALS Co., Ltd) experiments were carried out using the as-prepared catalyst film (deposited on a glassy carbon electrode) as the working electrode in a 0.1 M KOH alkaline electrolyte solution. A Pt wire and SCE were used as the counter and reference electrodes, respectively. Before the RRDE test, 0.1 M KOH electrolyte solution was saturated with pure oxygen gas (99.999%) for 30 min. Electrochemical characterization was conducted using a bi-potentiostat (Bio-Logic). 10 mV of the scan rate was swept from 0 to -0.8 V and a sufficient ring potential of 0.2 V was biased to oxidize the intermediate during the ORR. The collection efficiency was determined to be 0.412 in an Ar atmosphere using $10 \text{ mM K}_3[\text{Fe}(\text{CN})_6]$. This value is very close to its theoretical value of 0.42 . Hydrogen peroxide yields and the number of transferred electrons were calculated using the following equation:

$$\text{HO}_2^- (\%) = 200 \frac{\frac{I_r}{N}}{I_d + \frac{I_r}{N}}$$

$$n = 4 \frac{I_d}{I_d + \frac{I_r}{N}}$$

where I_r and I_d are the ring and disk current (A cm^{-2}) respectively and N is the experimentally determined collection efficiency of 0.412 .

Results and discussion

A brown aqueous suspension of graphene oxide (GO) was prepared by sonication of graphite oxide powder produced *via* chemical oxidation of pristine graphite using a modified Hummers method.^{58–62} During the oxidation process, a wide range of oxygen-containing functional groups are introduced, including hydroxyl and epoxy groups on the basal planes and carboxylic acid and ketone groups at the edges, which provide superior stability in aqueous media. The colloidal suspension of GO mainly comprises single-layer graphene nanosheets with a thickness of approximately 0.70 nm , as measured by atomic force microscopy (AFM) (Fig. S1 in the ESI†). The as-prepared GO suspension was mixed with a solution of dopamine (2 mg mL^{-1} of 10 mM Tris buffer, $\text{pH } 8.5$) at room temperature for 12 h to afford the polydopamine coated graphene nanosheet (G/pDopa). In agreement with the previous report, dopamine undergoes pH-triggered oxidative polymerization under alkaline conditions, resulting in simultaneous surface functionalization and reduction of the GO nanosheets.^{63,64} The resulting G/pDopa suspension showed a dark black color, reflecting the presence of pDopa and the partially restored conjugated aromatic structure. From the UV/vis spectra, we observed the appearance of a new peak at 280 nm , suggesting the characteristic absorption due to the dihydroxyindole from pDopa (Fig. S2 in the ESI†).⁶⁵ The NG catalysts were subsequently prepared by thermal annealing of as-prepared G/pDopa composites at different temperatures ranging from 600 to $1000 \text{ }^\circ\text{C}$ for 1 h in an Ar atmosphere. The resulting products were denoted as NG₆₀₀, NG₈₀₀ and NG₁₀₀₀, according to the reaction temperature. The thermal annealing approach caused atomic rearrangement leading to a highly ordered graphitic structure and the simultaneous incorporation of nitrogen atoms from the pDopa into the graphene matrix.⁶⁶ Moreover, it should be noted that the substituted-N atoms not only enhance the electrocatalytic activity for ORR, but also provide growth sites for metal oxide nanostructures. Hence, the MnO_x nanowires were grown on NG catalysts by mixing the manganese precursor, NaMnO_4 , in the NG suspension at various feed ratios (the ratio of NG to Mn precursor ranged from 0.5 to 10) followed by a mild thermal treatment at $85 \text{ }^\circ\text{C}$ for 1 h to afford the hybrid NG/ MnO_x catalyst.

The successful incorporation and nature of nitrogen-doping on the graphene nanosheets was identified by X-ray photoelectron spectroscopy (XPS) (Fig. 2). From the XPS survey spectra, we found the distinct evolution of nitrogen in G/pDopa and NG catalysts, which is absent in the initial GO nanosheets. A slight reduction of the oxygen peak in G/pDopa was also noticeable in pDopa attributable to the simultaneous surface functionalization and reduction of GO nanosheets consistent with the UV/vis measurements. Moreover, the oxidative polymerization of dopamine led to successful surface functionalization of GO nanosheets with pDopa at a total N-content of

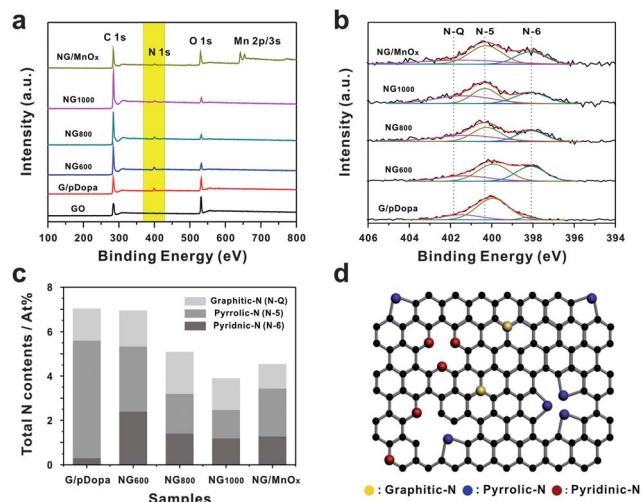


Fig. 2 (a) XPS survey spectra of various catalysts prepared in this study. (b) Deconvoluted high-resolution N 1s XPS spectra with three different N-configurations; N-6 (pyridinic-N, 398.1 eV), N-5 (pyrrolic-N, 399.9 eV), and N-Q (graphitic-N, 401.3 eV). (c) Total N content of G/pDopa, NG nanosheets based on the different pyrolysis temperatures and NG/MnO_x catalysts. (d) Three representative N-doping configurations on the NG nanosheet. NG/MnO_x (2 : 1) was used as a representative set.

7.0%. Upon thermal annealing of G/pDopa at various temperatures, the N-content decreased slightly to 6.95, 5.09 and 3.90% for NG₆₀₀, NG₈₀₀ and NG₁₀₀₀, respectively (Table S1 in the ESI†). These results support the evidence of dopamine induced N-doping on the graphene matrix, and also the possibility of simple modulation of the N-doping degree by controlling the pyrolysis temperature as similarly reported for other doping systems.^{52,56} The additional peak of Mn 2p/3s in the NG/MnO_x catalyst also indicated the formation of MnO_x nanostructures on the surface of the NG nanosheets.

The deconvoluted high-resolution N 1s XPS spectra further elucidated characteristic types of the N-doping on the graphene nanosheets (Fig. 2b–d and Table S2 in the ESI†). Specifically, three distinctive N-configurations were displayed, including pyridinic-N (N-6, 398.1 eV), pyrrolic-N (N-5, 399.9 eV) and graphitic-N (N-Q, 401.3 eV). Interestingly, we observed a predominant pyrrolic-N species due to the dihydroxyindole structure in pDopa.⁶⁵ Upon annealing at high temperatures, the majority of the pyrrolic-N species converted to both pyridinic-N and graphitic-N species, resulting in the fractions of each N-configuration changing accordingly (Fig. 2c).

As shown in Fig. 3a, the representative NG₈₀₀ catalyst exhibited a typical wrinkled and crumbled two-dimensional structure of the graphene sheet with lateral dimensions of 0.50–1.1 μm. This characteristic morphology can be attributed to defective structures formed upon exfoliation or the presence of doped nitrogen atoms. Transmission electron microscopy (TEM) revealed that the MnO_x in NG/MnO_x retained the morphology of the nanowire with an average diameter of 4.3 nm and a length of 30–80 nm on the surface of NG catalysts (Fig. 3b and c). Given the high density of the MnO_x nanowires formed

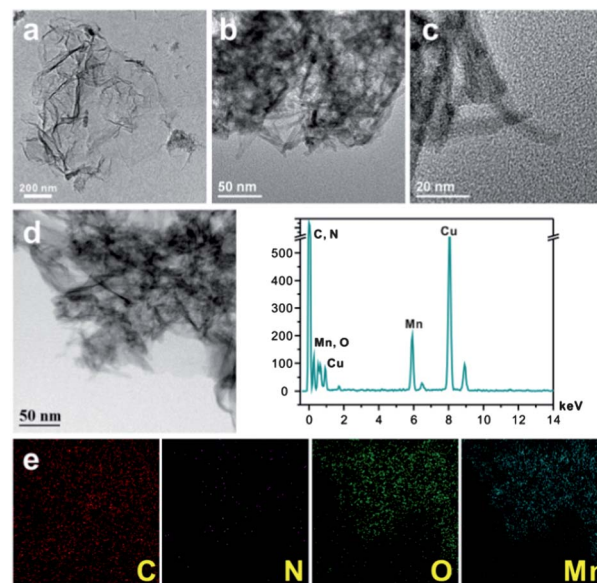


Fig. 3 Representative TEM images of (a) NG₈₀₀ and (b and c) NG/MnO_x catalysts with the MnO_x nanowires formed on the NG₈₀₀ substrate. (d and e) EDX elemental mapping analysis of the hybrid NG/MnO_x catalyst. Elements analyzed are noted at the corner of panel e.

on the surface of the NG, we can postulate that the N-doping effectively increased the interaction between the NG and the manganese precursor. Furthermore, the intimate interaction between graphene and nanowires allowed good dispersion of the MnO_x nanowires grown on the NG nanosheets, thus avoiding potential aggregation of nanowires during the electrocatalytic cycles. The EDX elemental mapping analysis demonstrated the presence of NG nanosheets by their distinctive elements such as C, O, and N as well as the presence of MnO_x nanowires by Mn and O elements (Fig. 3d and e). The crystalline phase of MnO_x nanowires was not further revealed by the selected area electron diffraction (SAED) pattern in the HR-TEM images, suggesting the amorphous nature of MnO_x nanowires formed on the NG nanosheets under mild reaction conditions. It has been suggested that the ORR activity of MnO_x largely depends on its crystalline structure and oxidation state; for example, Cho and co-workers reported that the higher density of surface defects in amorphous MnO_x supported on Ketjenblack carbon exhibited higher ORR activity by offering more active sites. Additionally, it allowed more binding configurations during the interaction of oxygen with the d-orbital of a metal ion for an effective ORR.⁶⁷

To explore the electrocatalytic activity during the ORR process of NG and NG/MnO_x catalysts, we obtained the rotating disk electrode (RDE) voltammograms in O₂-saturated 0.10 M KOH aqueous solution. As control experiments, non-doped graphene catalysts such as pristine GO, chemically reduced GO (CRGO) and thermally reduced GO (TRGO) were employed to verify the effect of N-doping for efficient ORR. Fig. 4 indicates a series of polarization curves at a constant rotating rate of 1600 rpm and quantitative evaluation in terms of the onset potential

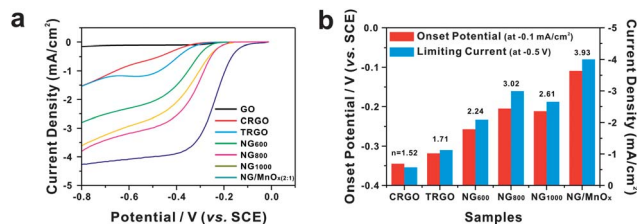


Fig. 4 (a) Polarization curves of all NG and NG/MnO_x electrocatalysts prepared in the study. The electrochemical activities were compared with control sets of the pristine GO, chemically reduced GO (CRGO) and thermally reduced GO (TRGO). (b) Comparison of the onset potential and limiting current density of each catalyst with the electron transfer number (n) based on the Koutecky–Levich equation determined by RDE experiments. All electrochemical tests were acquired at a rotation rate of 1600 rpm and a scan rate of 10 mV s⁻¹ in O₂-saturated 0.10 M KOH electrolyte solution. The onset potential was measured at -0.1 mA cm⁻² and the limiting current was measured at -0.50 V (vs. SCE).

(V) and kinetic limiting current density (J_k) on the basis of the RDE measurements. The electron transfer number (n) of each catalyst was also calculated during the ORR process from the RDE results based on the Koutecky–Levich (K–L) equation. The K–L plot relates the current density (i) with the rotation rate of the electrode (ω) to determine both the kinetic current (i_k) and the number of transferred electrons (n) involved in the ORR.^{68,69} Unlike pristine GO, both CRGO and TRGO showed an improved performance compared to pristine GO, while both reduced GOs displayed negligible ORR activity with a dominant two-step, two-electron ORR pathway. Meanwhile, the N-doped graphene catalysts displayed considerably enhanced electrocatalytic activity. Among all the NG samples, the NG₈₀₀ showed the most positive onset potential at -0.20 V and the highest limiting current density of -3.0 mA cm⁻² (Fig. S3 in the ESI†). It is proposed that this result is closely related to the type of N-configuration in NG₈₀₀, as determined by high-resolution XPS, in which a relatively high portion of graphitic-N species effectively contributed to the enhanced ORR catalytic activity (*i.e.*, 37.3% of NG₈₀₀ vs. 23.3% of NG₆₀₀). Although there has been significant progress in the synthesis and applications of N-doped carbon nanomaterials for ORR, which types of nitrogen are active sites for ORR is still controversial as its contribution to catalytic activity is not well defined. The pyridinic-N sites have widely received credit as catalytic active sites for ORR because of the delocalization of the π -electrons from pyridinic-N.⁷⁰ Additionally, XPS experiments showed that highly catalytic carbon materials usually retain a large amount of pyridinic-N.^{71–73} In contrast, a recent study by Knights and co-workers reported that the electronegative graphitic-N species reduce the electron density on the adjacent carbon nuclei, which helps electrons transfer from the adjacent C to N atoms.⁷⁴ This electron transfer process not only facilitates O₂ dissociation on the adjacent C atoms, but also helps to form a strong chemical bond between O and C. In a separate study by Ruoff and co-workers,⁵³ they investigated the electrocatalytic activity based on the graphitic-N content which determined the limiting current density, while the pyridinic-N content improved the onset

potential for ORR. In accordance with these claims, we observed that the graphitic-N species played the most important role in ORR activity by facilitating oxygen reduction in the NG nanosheets. Although the N-doping on graphene nanosheets significantly increased the ORR activity compared to the non-doped counterparts, n for all NG catalysts, determined from the K–L plot, was in the range of 2.2–3.0, indicating both two- and four-electron reduction pathways taking place together.

The limited catalytic activities of NG catalysts can be complemented with controlled growth of MnO_x nanowires on the NG nanosheets as clearly evidenced in Fig. 4. Here NG₈₀₀ was employed as a substrate owing to its high electrochemical activity among the prepared NG nanosheets. Furthermore, the relative amount of active material can be tuned with respect to the NG catalyst in order to optimize the electrochemical performance. The NG/MnO_x hybrid catalysts were prepared by varying the feed ratio of NG to Mn precursor from 0.5 to 10. The resulting hybrid NG/MnO_x catalyst was denoted as NG/MnO_{x(0.5:1)}, NG/MnO_{x(2:1)} and NG/MnO_{x(10:1)} depending on the relative ratio of the NG nanosheets and MnO_x content. Thermogravimetric analysis (TGA) provided the relative amount of MnO_x that ranged between 62.8 (NG/MnO_{x(0.5:1)}), 31.3 (NG/MnO_{x(2:1)}) and 19.4% (NG/MnO_{x(10:1)}) (Fig. S4 in the ESI†). After careful evaluation of their electrocatalytic behaviors, the hybrid NG/MnO_{x(2:1)} had the best performance among all samples. For example, the NG/MnO_{x(2:1)} catalyst exhibited significantly higher catalytic activity than NG₈₀₀ and TRGO/MnO_{x(2:1)} with an onset potential of -0.13 V and a limiting current density of -4.0 mA cm⁻². In addition, it demonstrated a direct four-electron reduction pathway ($n = 3.93$), similar to commercial Pt/C catalysts (Fig. S5 and S6 in the ESI†). This suggests that a fine balance between the graphene supports and amounts of catalytic materials is also an important factor in determining the electrocatalytic activity. Moreover, the synergistic coupling effect of N-doping on carbon supports and MnO_x active materials has proven to effectively improve the catalytic activity for ORR.

To further verify the ORR catalytic pathways with the optimized hybrid NG/MnO_{x(2:1)} catalysts, rotating ring-disk electrode (RRDE) measurements were performed to monitor the formation of peroxide species (HO₂⁻) during the ORR process. Fig. 5a shows the disk and ring currents recorded at 1600 rpm in 0.10 M KOH for the NG₈₀₀ and NG/MnO_{x(2:1)} in comparison with commercial Pt/C catalysts. The NG/MnO_{x(2:1)} exhibited a higher disk current (oxygen reduction) and a smaller ring current (peroxide oxidation) than the NG₈₀₀ catalyst. The percentage of peroxide species with respect to the total oxygen reduction products and the electron transfer number (n) calculated from the RRDE curves are presented in Fig. 5b. The measured HO₂⁻ yields are around 10% over the entire potential range of -0.1 to -0.8 V for the NG/MnO_{x(2:1)} catalyst; this value is significantly lower than that of the NG catalyst, which is near 60%. The average electron transfer number, n , was ~3.9 from -0.1 to -0.8 V for the hybrid that is close to a commercial Pt/C catalyst. This is consistent with the result obtained from the K–L plot based on the RDE measurements, suggesting that the hybrid NG/MnO_{x(2:1)} catalyst can undergo a one-step, direct 4-electron ORR pathway with a low yield of the peroxide intermediate.

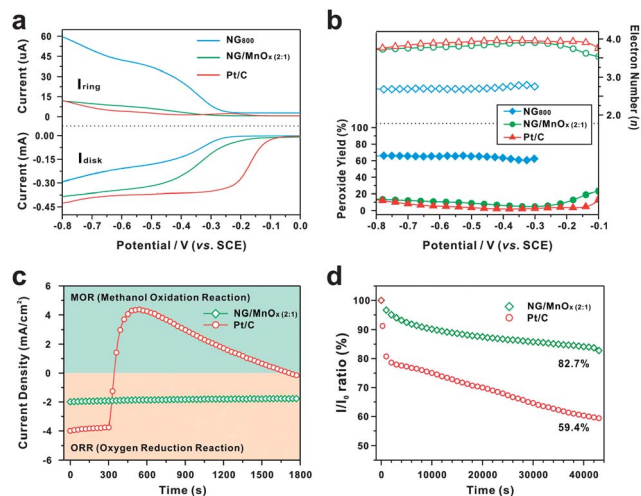


Fig. 5 (a) RRDE experiments of NG, NG/MnO_{x(2:1)} and commercial 20 wt% Pt/C catalysts in O₂-saturated 0.10 M KOH aqueous solution at 1600 rpm. (b) The plot of the peroxide yields (%) and the electron transfer number (*n*) of electrocatalysts. (c) Characterization of the methanol tolerance of NG/MnO_{x(2:1)} and 20 wt% Pt/C catalysts. 3 M methanol was injected into the electrolyte at 300 s. (d) Chronoamperometric responses of NG/MnO_{x(2:1)} and Pt/C catalysts at -0.5 V (vs. SCE) in an O₂-saturated 0.1 M KOH solution with 1600 rpm.

Finally, the methanol crossover effect and durability of all catalysts were assessed using chronoamperometric measurements (Fig. 5c and d). The chronoamperometric response of the NG/MnO_{x(2:1)} catalyst remained stable even after methanol injection at 300 s, indicating no influence from methanol crossover. In clear contrast, the current density of the commercial Pt/C catalyst dramatically jumped to a positive value after methanol injection, suggesting that the methanol oxidation reaction (MOR) occurs on the surface of the Pt catalysts. The durability test was also conducted at a constant reduction potential of -0.5 V. After 12 h of operation, the NG/MnO_{x(2:1)} hybrid catalyst showed a marginal activity loss of 17.3%, whereas Pt/C lost nearly 40.6% of its initial activity. This confirmed that the hybrid NG/MnO_x electrocatalyst has a much better stability for ORR in an alkaline environment.

Conclusions

In summary, a hybrid electrocatalyst of amorphous manganese oxide nanowires supported on nitrogen-doped graphene nanosheets (NG/MnO_x) was developed for an efficient ORR. A mussel-inspired dopamine moiety was employed as the source of nitrogen doping onto graphene nanosheets, which was subsequently used as the growth site for the amorphous MnO_x nanowires on the surface of NG. The hybrid NG/MnO_x catalyst exhibits excellent catalytic activity with a direct four-electron pathway in ORR. Furthermore, the hybrid electrocatalyst possesses superior stability and gives a low yield of peroxide compared to commercial Pt/C catalysts. We suggest that the synergistic coupling effect of N-doping on carbon supports and

active MnO_x nanowires by an electronic conductive substrate can effectively improve the catalytic activity for ORR.

Acknowledgements

This research was supported by the National Research Foundation of Korea (NRF) grant (2012R1A1A2040782).

Notes and references

- 1 M. Winter and R. J. Brodd, *Chem. Rev.*, 2004, **104**, 4245–4270.
- 2 A. S. Arico, P. Bruce, B. Scrosati, J.-M. Tarascon and W. van Schalkwijk, *Nat. Mater.*, 2005, **4**, 366–377.
- 3 N. S. Lewis and D. G. Nocera, *Proc. Natl. Acad. Sci. U. S. A.*, 2006, **103**, 15729–15735.
- 4 Y.-G. Guo, J.-S. Hu and L.-J. Wan, *Adv. Mater.*, 2008, **20**, 2878–2887.
- 5 M. S. Whittingham, *Chem. Rev.*, 2004, **104**, 4271–4302.
- 6 P. G. Bruce, S. A. Freunberger, L. J. Hardwick and J.-M. Tarascon, *Nat. Mater.*, 2012, **11**, 19–29.
- 7 M. Armand and J. M. Tarascon, *Nature*, 2008, **451**, 652–657.
- 8 J.-S. Lee, S. T. Kim, R. Cao, N.-S. Choi, M. Liu, K. T. Lee and J. Cho, *Adv. Energy Mater.*, 2011, **1**, 34–50.
- 9 F. Cheng and J. Chen, *Chem. Soc. Rev.*, 2012, **41**, 2172–2192.
- 10 B. C. H. Steele and A. Heinzl, *Nature*, 2001, **414**, 345–352.
- 11 A. A. Gewirth and M. S. Thorum, *Inorg. Chem.*, 2010, **49**, 3557–3566.
- 12 V. R. Stamenkovic, B. Fowler, B. S. Mun, G. Wang, P. N. Ross, C. A. Lucas and N. M. Marković, *Science*, 2007, **315**, 493–497.
- 13 S. Wang, D. Yu and L. Dai, *J. Am. Chem. Soc.*, 2011, **133**, 5182–5185.
- 14 Y. Liang, H. Wang, J. Zhou, Y. Li, J. Wang, T. Regier and H. Dai, *J. Am. Chem. Soc.*, 2012, **134**, 3517–3523.
- 15 J. Suntivich, H. A. Gasteiger, N. Yabuuchi, H. Nakanishi, J. B. Goodenough and Y. Shao-Horn, *Nat. Chem.*, 2011, **3**, 546–550.
- 16 V. Stamenkovic, B. S. Mun, K. J. J. Mayrhofer, P. N. Ross, N. M. Markovic, J. Rossmeisl, J. Greeley and J. K. Nørskov, *Angew. Chem., Int. Ed.*, 2006, **45**, 2897–2901.
- 17 R. Srivastava, P. Mani, N. Hahn and P. Strasser, *Angew. Chem., Int. Ed.*, 2007, **46**, 8988–8991.
- 18 Z. Peng and H. Yang, *J. Am. Chem. Soc.*, 2009, **131**, 7542–7543.
- 19 M. Arenz, K. J. J. Mayrhofer, V. Stamenkovic, B. B. Blizanac, T. Tomoyuki, P. N. Ross and N. M. Markovic, *J. Am. Chem. Soc.*, 2005, **127**, 6819–6829.
- 20 A. Kowal, M. Li, M. Shao, K. Sasaki, M. B. Vukmirovic, J. Zhang, N. S. Marinkovic, P. Liu, A. I. Frenkel and R. R. Adzic, *Nat. Mater.*, 2009, **8**, 325–330.
- 21 A. Morozan, B. Jousselme and S. Palacin, *Energy Environ. Sci.*, 2011, **4**, 1238–1254.
- 22 Y. Liang, Y. Li, H. Wang, J. Zhou, J. Wang, T. Regier and H. Dai, *Nat. Mater.*, 2011, **10**, 780–786.
- 23 Y. Zheng, Y. Jiao, J. Chen, J. Liu, J. Liang, A. Du, W. Zhang, Z. Zhu, S. C. Smith, M. Jaroniec, G. Q. Lu and S. Z. Qiao, *J. Am. Chem. Soc.*, 2011, **133**, 20116–20119.

- 24 M. Jahan, Q. Bao and K. P. Loh, *J. Am. Chem. Soc.*, 2012, **134**, 6707–6713.
- 25 R. Liu, D. Wu, X. Feng and K. Müllen, *Angew. Chem., Int. Ed.*, 2010, **49**, 2565–2569.
- 26 K. Ai, Y. Liu, C. Ruan, L. Lu and G. Lu, *Adv. Mater.*, 2013, **25**, 998–1003.
- 27 J. E. Post, *Proc. Natl. Acad. Sci. U. S. A.*, 1999, **96**, 3447–3454.
- 28 L. Mao, D. Zhang, T. Sotomura, K. Nakatsu, N. Koshihara and T. Ohsaka, *Electrochim. Acta*, 2003, **48**, 1015–1021.
- 29 M. S. El-Deab and T. Ohsaka, *Angew. Chem., Int. Ed.*, 2006, **45**, 5963–5966.
- 30 F. H. B. Lima, M. L. Calegaro and E. A. Ticianelli, *Electrochim. Acta*, 2007, **52**, 3732–3738.
- 31 Y. Tan, C. Xu, G. Chen, X. Fang, N. Zheng and Q. Xie, *Adv. Funct. Mater.*, 2012, **22**, 4584–4591.
- 32 Y. Gorlin, C.-J. Chung, D. Nordlund, B. M. Clemens and T. F. Jaramillo, *ACS Catal.*, 2012, **2**, 2687–2694.
- 33 J.-S. Lee, T. Lee, H.-K. Song, J. Cho and B.-S. Kim, *Energy Environ. Sci.*, 2011, **4**, 4148–4154.
- 34 H. Kim and B. N. Popov, *J. Electrochem. Soc.*, 2003, **150**, D56–D62.
- 35 E. Raymundo-Piñero, V. Khomenko, E. Frackowiak and F. Béguin, *J. Electrochem. Soc.*, 2005, **152**, A229–A235.
- 36 L. L. Zhang, T. Wei, W. Wang and X. S. Zhao, *Micropor. Mesopor. Mater.*, 2009, **123**, 260–267.
- 37 K. S. Novoselov, A. K. Geim, S. V. Morozov, D. Jiang, Y. Zhang, S. V. Dubonos, I. V. Grigorieva and A. A. Firsov, *Science*, 2004, **306**, 666–669.
- 38 S. Stankovich, D. A. Dikin, G. H. B. Dommett, K. M. Kohlhaas, E. J. Zimney, E. A. Stach, R. D. Piner, S. T. Nguyen and R. S. Ruoff, *Nature*, 2006, **442**, 282–286.
- 39 A. K. Geim and K. S. Novoselov, *Nat. Mater.*, 2007, **6**, 183–191.
- 40 S. Wang, L. Zhang, Z. Xia, A. Roy, D. W. Chang, J.-B. Baek and L. Dai, *Angew. Chem., Int. Ed.*, 2012, **51**, 4209–4212.
- 41 S. Yang, L. Zhi, K. Tang, X. Feng, J. Maier and K. Müllen, *Adv. Funct. Mater.*, 2012, **22**, 3634–3640.
- 42 J. Wu, W. Pisula and K. Müllen, *Chem. Rev.*, 2007, **107**, 718–747.
- 43 S. Guo, D. Wen, Y. Zhai, S. Dong and E. Wang, *ACS Nano*, 2010, **4**, 3959–3968.
- 44 H. Wang, L.-F. Cui, Y. Yang, H. Sanchez Casalongue, J. T. Robinson, Y. Liang, Y. Cui and H. Dai, *J. Am. Chem. Soc.*, 2010, **132**, 13978–13980.
- 45 Y. Sun, Q. Wu and G. Shi, *Energy Environ. Sci.*, 2011, **4**, 1113–1132.
- 46 Z.-S. Wu, Y. Sun, Y.-Z. Tan, S. Yang, X. Feng and K. Müllen, *J. Am. Chem. Soc.*, 2012, **134**, 19532–19535.
- 47 Y. Zhao, C. Hu, Y. Hu, H. Cheng, G. Shi and L. Qu, *Angew. Chem., Int. Ed.*, 2012, **51**, 11371–11375.
- 48 Z.-S. Wu, A. Winter, L. Chen, Y. Sun, A. Turchanin, X. Feng and K. Müllen, *Adv. Mater.*, 2012, **24**, 5130–5135.
- 49 Z.-S. Wu, S. Yang, Y. Sun, K. Parvez, X. Feng and K. Müllen, *J. Am. Chem. Soc.*, 2012, **134**, 9082–9085.
- 50 K. Parvez, S. Yang, Y. Hernandez, A. Winter, A. Turchanin, X. Feng and K. Müllen, *ACS Nano*, 2012, **6**, 9541–9550.
- 51 L. Qu, Y. Liu, J.-B. Baek and L. Dai, *ACS Nano*, 2010, **4**, 1321–1326.
- 52 X. Li, H. Wang, J. T. Robinson, H. Sanchez, G. Diankov and H. Dai, *J. Am. Chem. Soc.*, 2009, **131**, 15939–15944.
- 53 L. Lai, J. R. Potts, D. Zhan, L. Wang, C. K. Poh, C. Tang, H. Gong, Z. Shen, J. Lin and R. S. Ruoff, *Energy Environ. Sci.*, 2012, **5**, 7936–7942.
- 54 S. Wang, D. Yu, L. Dai, D. W. Chang and J.-B. Baek, *ACS Nano*, 2011, **5**, 6202–6209.
- 55 Z. Lin, M.-k. Song, Y. Ding, Y. Liu, M. Liu and C.-p. Wong, *Phys. Chem. Chem. Phys.*, 2012, **14**, 3381–3387.
- 56 Z.-H. Sheng, L. Shao, J.-J. Chen, W.-J. Bao, F.-B. Wang and X.-H. Xia, *ACS Nano*, 2011, **5**, 4350–4358.
- 57 H. M. Jeong, J. W. Lee, W. H. Shin, Y. J. Choi, H. J. Shin, J. K. Kang and J. W. Choi, *Nano Lett.*, 2011, **11**, 2472–2477.
- 58 W. S. Hummers and R. E. Offeman, *J. Am. Chem. Soc.*, 1958, **80**, 1339.
- 59 D. Li, M. B. Muller, S. Gilje, R. B. Kaner and G. G. Wallace, *Nat. Nanotechnol.*, 2008, **3**, 101–105.
- 60 S. Park and R. S. Ruoff, *Nat. Nanotechnol.*, 2009, **4**, 217–224.
- 61 T.-K. Hong, D. W. Lee, H. J. Choi, H. S. Shin and B.-S. Kim, *ACS Nano*, 2010, **4**, 3861–3868.
- 62 T. Lee, T. Yun, B. Park, B. Sharma, H.-K. Song and B.-S. Kim, *J. Mater. Chem.*, 2012, **22**, 21092–21099.
- 63 S. M. Kang, S. Park, D. Kim, S. Y. Park, R. S. Ruoff and H. Lee, *Adv. Funct. Mater.*, 2011, **21**, 108–112.
- 64 L. Q. Xu, W. J. Yang, K.-G. Neoh, E.-T. Kang and G. D. Fu, *Macromolecules*, 2010, **43**, 8336–8339.
- 65 H. Lee, S. M. Dellatore, W. M. Miller and P. B. Messersmith, *Science*, 2007, **318**, 426–430.
- 66 H. Hwang, P. Joo, M. S. Kang, G. Ahn, J. T. Han, B.-S. Kim and J. H. Cho, *ACS Nano*, 2012, **6**, 2432–2440.
- 67 J.-S. Lee, G. S. Park, H. I. Lee, S. T. Kim, R. Cao, M. Liu and J. Cho, *Nano Lett.*, 2011, **11**, 5362–5366.
- 68 J. Koutecky and V. Levich, *Zh. Fiz. Khim.*, 1958, **32**, 1565–1575.
- 69 S. Treimer, A. Tang and D. C. Johnson, *Electroanalysis*, 2002, **14**, 165–171.
- 70 R. P. O’Hayre, S.-W. Cha, W. Colella and F. B. Prinz, *Fuel Cell Fundamentals*, John Wiley & Sons, New York, 2006.
- 71 S. Kundu, T. C. Nagaiah, W. Xia, Y. Wang, S. V. Dommele, J. H. Bitter, M. Santa, G. Grundmeier, M. Bron, W. Schuhmann and M. Muhler, *J. Phys. Chem. C*, 2009, **113**, 14302–14310.
- 72 K. R. Lee, K. U. Lee, J. W. Lee, B. T. Ahn and S. I. Woo, *Electrochem. Commun.*, 2010, **12**, 1052–1055.
- 73 C. V. Rao, C. R. Cabrera and Y. Ishikawa, *J. Phys. Chem. Lett.*, 2010, **1**, 2622–2627.
- 74 D. Geng, Y. Chen, Y. Chen, Y. Li, R. Li, X. Sun, S. Ye and S. Knights, *Energy Environ. Sci.*, 2011, **4**, 760–764.